arXiv:2403.09013v1 [cond-mat.mtrl-sci] 14 Mar 2024

Impacts of Point Defects on Shallow Doping in Cubic Boron Arsenide: A First Principles Study

Shuxiang Zhou[1a)] and Zilong Hua[1], Kaustubh K. Bawane[1], Hao Zhou[2], and Tianli Feng[2]
[1] *Idaho National Laboratory, Idaho Falls, Idaho 83415, USA*
[2] *Department of Mechanical Engineering, University of Utah, Salt Lake City, Utah 84112, USA*

Cubic boron arsenide (BAs) stands out as a promising material for advanced electronics, thanks to its exceptional thermal conductivity and ambipolar mobility. However, effective control of p- and n-type doping in BAs poses a significant challenge, mostly as a result of the influence of defects. In the present study, we employed density functional theory to explore the impacts of the common point defects and impurity on p-type doping $\mathrm{Be_B}$ and $\mathrm{Si_{As}}$, and n-type doping $\mathrm{Si_B}$ and $\mathrm{Se_{As}}$. We find that the most favorable points defects formed by C, O, and Si are $\mathrm{C_{As}}$, $\mathrm{O_BO_{As}}$, $\mathrm{Si_{As}}$, $\mathrm{C_{As}Si_B}$, and $\mathrm{O_BSi_{As}}$, which have formation energies of less than 1.5 eV. For p-type doping, C, O, and Si impurities do not harm the shallow state of $\mathrm{Be_B}$ doping, while only O impurity detrimentally affects $\mathrm{Si_{As}}$ doping. However for n-type dopings, C, O, and Si impurities are all harmful. Interestingly, the antisite defect pair $\mathrm{As_BB_{As}}$ benefits both p- and n-type doping. The doping limitation analysis presented in this study can potentially pave the way for strategic development in the area of BAs-based electronics.

Over the last decade, cubic boron arsenide (BAs) has attracted an extremely high level of research interest, due to its exceptional thermal conductivity and ambipolar mobility. The thermal conductivity of BAs (i.e., ∼1300 W/mK at room temperature, which is only surpassed by diamond for bulk materials) was first predicted via theory[1–3], then validated by experiments[4–6]. The simultaneously high room-temperature electron and hole mobilities were also predicted by theory[7] and later confirmed through recent experiments[8,9]. Beyond its remarkable transport properties, BAs is applicable to existing III–V semiconductor technology[10], and has an electronic structure similar to that of Si, but with a wider band gap[11]. These attributes position BAs as a promising material for advanced electronics and efficient heat management.

One critical need in high-performance electronic applications relates to the development of methodologies to control p- and n-type doping, in order to generate the desired ionizable delocalized (shallow) impurity states[12]. To accomplish this, the behaviors of defects such as intrinsic defects and impurities must be comprehensively understood. Despite the successful synthesis of millimeter-sized BAs crystals, achieved via the chemical vapor transport method[13–16], a substantial variance is still observed in the measured thermal properties of BAs[5,17–19]. Coupled with the observation of p-type semiconducting behavior[15,19,20], these results indicate the presence of intrinsic defects and impurities in BAs samples. While extensive research[8,21–25] has been performed on the thermal conductivity reduction caused by intrinsic defects and impurities, comparably less emphasis has been placed on comprehending how intrinsic defects and impurities affect electronic properties. Notably, first principles calculations[21,26,27] were utilized to explore the formation of intrinsic defects, identifying the antisite pair $\mathrm{As_BB_{As}}$ as being the most prevalent intrinsic defect type. However, the antisite pair $\mathrm{As_BB_{As}}$ is usually neutral and thus cannot explain the observed p-type semiconducting behavior. Theoretical studies attribute the p-type semiconducting behavior of BAs to impurities, such as Si, C, and H[26,27], whereas recent experiments have validated the presence of Si, C, O, H, Te, and I impurities in BAs[24].

Furthermore, the first principles calculations identified specific dopants (e.g., $\mathrm{Be_B}$ and $\mathrm{Si_{As}}$ for p-type, and $\mathrm{Si_B}$ and $\mathrm{Se_{As}}$ for n-type) characterized as shallow dopants[26,27]. A high p-dopability of BAs is also reported[27,28]. However, the behaviors of shallow dopants can be influenced by point defects, as the aforementioned impurities can solely induce p-type behavior. Notably, how various point defects influence the behaviors of shallow dopants have never comprehensively been investigated. Thus, for the present work, we conduct a detailed thermodynamic analysis demonstrating the interaction between point defects and shallow dopants utilizing density functional theory (DFT).

In the present work, the DFT calculations were carried out using the projector augmented-wave method[29,30], as implemented in the Vienna ab initio Simulation Package code[31,32]. The employed exchange correlation functional was the generalized gradient approximation (GGA) as formulated by Perdew, Burke, and Ernzerhof functional revised for solids (PBEsol)[33]. Notably, previous DFT calculations[26,27] utilized the Heyd-Scuseria-Ernzerhof (HSE) functional[34], which, as compared to the PBE functional, can more accurately predict the band gap but has a considerably higher computational cost, limiting its use in exploring different configurations involving both dopants and point defects. In Sec. II of the Supplemental Materials (SM)[35], we compute the formation energy of p- and n-type dopants using PBEsol, and comparable results were obtained between PBEsol and HSE results from Ref.[26,27]. We therefore use PBEsol

---

[a)] Electronic mail: shuxiang.zhou@inl.gov

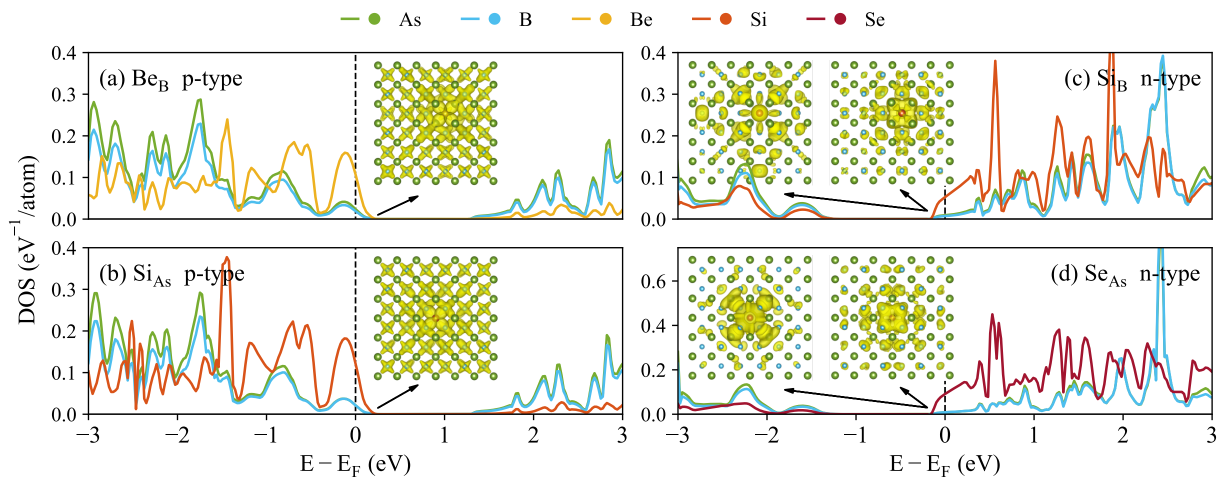

FIG. 1. Calculated electronic DOS of BAs doped by (a) $\mathrm{Be_B}$, (b) $\mathrm{Si_{As}}$, (c) $\mathrm{Si_B}$, and (d) $\mathrm{Se_{As}}$. The colored curves represent the DOS projection on different atoms. The inset figures are the isosurfaces of charge density near the CBM or VBM (<0.1 eV). The differently colored atoms represent different species.

throughout this work. For all calculations, spin polarization, a plane-wave cutoff energy of 700 eV, and an energy convergence criterion of 10^{-6} eV were applied. For the defect calculations, a $3\times3\times3$ supercell of the conventional cubic cell (216 atoms) and a $2\times2\times2$ Γ-centered k-point mesh were employed, as used by previous study[12]. The total charge of the defected systems was kept neutral. The relaxed lattice parameter of the conventional cubic cell of BAs was 4.778 Å.

The key properties computed are the formation energies and the isosurfaces of charge density. The formation energy values quantified the ease of defect formation, while the isosurfaces of charge density were employed to visualize the spatial localization of impurity states. The formation energy E_f of a given defect (or dopant) X is calculated as:

$$E_f(X) = E(X) - E_0 - \sum_i n_i^X (E_i + \mu_i) \qquad (1)$$

where E_0 is the total energy of the pristine system, $E(X)$ is the total energy of the defected system, n_i^X is the change in the number of atoms of species i due to defect X (positive if atoms are added, negative if atoms are removed), E_i is the energy per atom in the elemental phase, and μ_i is the chemical potential of species i. The elemental phases of species B, As, C, O, Si, Be, and Se were considered using α-B, α-As, graphene, oxygen gas, Si in the diamond structure, Be in the hexagonal close-packed structure, and α-Se, respectively. For all species i, $\mu_i \leq 0$. Furthermore, for all impurity atoms and dopants, μ_i was approximated as zero. The values of μ_B and μ_{As} depend on the growth condition involved: in the As-rich condition, $\mu_{As} = 0$; otherwise, $\mu_B = 0$ in the B-rich condition. Additionally, μ_B and μ_{As} are restricted by the equilibrium condition $\mu_B + \mu_{As} = \Delta H_{BAs}$, where ΔH_{BAs} is the formation enthalpy of BAs. Throughout this work, we use the As-rich condition, following Ref.[21]. Nevertheless, the PBEsol-predicted value of ΔH_{BAs} is merely -0.056 eV, meaning that the differences in μ_B (or μ_{As}) between As- and B-rich conditions only total -0.056 eV, which is trivial. Assuming a defect X is already present in the system, the formation energy of a dopant D can be determined using the formula $E_f^X(D) = E_f(D\text{-}X) - E_f(X)$, where $E_f(D\text{-}X)$ is the formation energy when both the dopant D and the defect X coexist (see Sec. I of SM[35] for more details). Comparing $E_f^X(D)$ against $E_f(D)$ affords insight into whether the defect X is advantageous for the formation of the dopant D. The isosurfaces of charge density were visualized using the VESTA package[36]. Additionally, $\mathrm{X_Y}$ was used to represent a substitutional X atom in the Y site.

Here we begin by identifying the dopants. HSE calculations[26,27] suggest p-type dopants $\mathrm{Be_B}$ and $\mathrm{Si_{As}}$ and n-type dopants $\mathrm{Se_{As}}$ and $\mathrm{Si_B}$ are shallow dopants with low formation energy. Using PBEsol (see Sec. II of SM[35] for more details), our results also confirm that the formation energies of $\mathrm{Be_B}$ (0.15 eV), $\mathrm{Si_{As}}$ (0.42 eV), $\mathrm{Si_B}$ (1.76 eV), and $\mathrm{Se_{As}}$ (1.47 eV) are the lowest among the computed dopants. Note that for p-type doping ($\mathrm{Be_B}$ and $\mathrm{Si_{As}}$), the formation energy is substantially lower than that for n-type doping ($\mathrm{Se_{As}}$ and $\mathrm{Si_B}$), thus supporting the notion that p-type doping occurs more readily in BAs than n-type[26,27]. In addition, the electronic density of states (DOS) and isosurface of charge density were computed for $\mathrm{Be_B}$, $\mathrm{Si_{As}}$, $\mathrm{Si_B}$, and $\mathrm{Se_{As}}$ (see Fig. 1). For $\mathrm{Be_B}$ and $\mathrm{Si_{As}}$, while the Fermi level E_F slightly shifts into the valence bands, there are three-fold degenerated bands at VBM, and their isosurfaces of charge density exhibit strong spatially delocalized natures, directly revealing $\mathrm{Be_B}$ and $\mathrm{Si_{As}}$ to be shallow acceptor impurities. For $\mathrm{Se_{As}}$ and $\mathrm{Si_B}$, E_F slightly shifts into the conduction

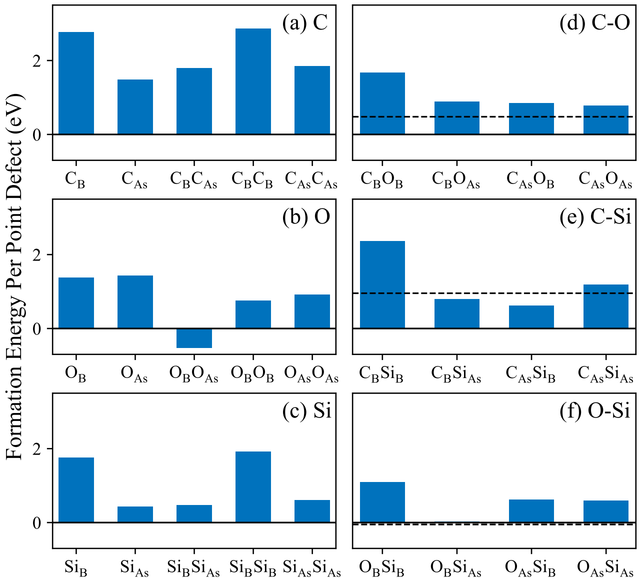

FIG. 2. Calculated formation energy per point defect formed by (a) C, (b) O, (c) Si, (d) C and O, (e) C and Si, and (f) Si and O, in pristine BAs. The dashed lines in (d), (e), and (f) indicate the mean value of the formation energy per point defect of isolated (d) C_{As} and O_BO_{As}, (e) C_{As} and Si_{As}, and (f) O_BO_{As} and Si_{As}, respectively.

bands. Two bands with moderate delocalization are observed: one with its bottom at CBM (inset figures on the left) and the other with its bottom within 0.1 eV of CBM (inset figures on the right), showing that both Se_{As} and Si_B are shallow donor impurities. Therefore, Be_B, Si_{As}, Si_B, and Se_{As} were selected for further investigation regarding the influence of point defects, in terms of four different cases: p- and n-type dopants on both B and As sites.

Given the multitude of configurations involving different species and atom sites for point defects, it is imperative to select the most representative ones. First, we considered C, O, and Si as the impurity elements, due to their high concentration as substitutional impurities, as reported in Ref.[24]. Secondly, we restricted our consideration to single point defects and point defect pairs in the first nearest neighbor. For each situation, only the point defect with the lowest formation energy was investigated further. Fig. 2 presents the calculation results. Panels (a), (b), and (c) reflect situations in which individual C, O, and Si impurities existed, respectively, whereas panels (d), (e), and (f) reflect situations in which combinations of C and O, C and Si, and O and Si impurities coexisted, respectively. Please note that, for a direct comparison, the y-axis value is the formation energy per point defect, meaning that the formation energy of defect pairs is divided by two. From Fig. 2(a)–(c), C_{As}, O_BO_{As}, and Si_{As} are the most favorable point defects when C, O, and Si are the only impurity elements, respectively. In Fig. 2(d), rather than forming defect pairs, C and O impurities are more likely to form isolated C_{As} and O_BO_{As} (indicated by the dashed line). In contrast, C and Si atoms are more likely to form $C_{As}Si_B$, as opposed to isolated C_{As} and Si_{As} (indicated by the dashed line). When O and Si coexist, the formation energy per point defect of O_BSi_{As} is 0.04 eV, and the mean formation energy per point defect of O_BO_{As} and Si_{As} is -0.10 eV (see Fig. 2(f)). Given the small difference (0.14 eV) between these two values, we exceptionally count in O_BSi_{As} into further investigation. To summarize, we selected C_{As}, O_BO_{As}, Si_{As}, $C_{As}Si_B$, and O_BSi_{As} as representative point defects of impurity.

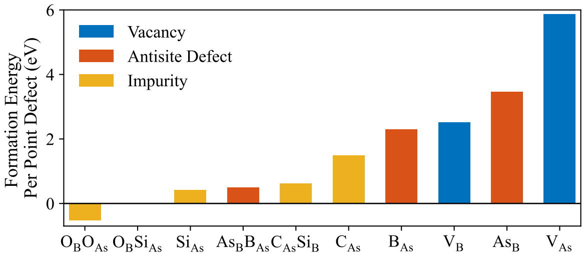

FIG. 3. Calculated formation energy of selected single point defects and point defect pairs. The obtained results are organized in ascending order.

We also examine the intrinsic point defects, including antisite single defects As_B and B_{As}, antisite defect pair As_BB_{As}, and single vacancies V_B and V_{As}. The formation energy per point defect for each of these intrinsic defects is plotted alongside the selected point defects of impurities, moving from the smallest formation energy (left) to the largest (right) (see Fig. 3). Certainly, only the antisite defect pair As_BB_{As} has a formation energy comparable to that of the selected point defects of impurity. Thus, we will discuss a total of six types of point defects, including the aforementioned five selected types of impurities plus As_BB_{As}, where the formation energies per point defect are all less than 1.5 eV.

Finally, we discuss the impact of these common point defects (As_BB_{As}, C_{As}, O_BO_{As}, Si_{As}, C_{As}, Si_B, and O_BSi_{As}) on both the formation energy and the electronic characteristics of shallow dopants Be_B, Si_{As}, Si_B, and Se_{As}. Please note that, with respect to Si_{As} being regarded as a p-type dopant, Si_{As} itself is no longer categorized as a point defect of impurity, while $C_{As}Si_B$ and O_BSi_{As} continue to be considered as impurities due to the presence of C and O. In Sec. IV of SM[35], we consider additional point defects As_B, B_{As}, and N_{As}, despite their potential lack of favorability within the BAs system. When different point defects are present, the dopants may occupy various atom sites. For each combination of point defect and dopant, all possible dopant sites within 6Å of the point defects are computed. Sec. III of SM tabulates the detailed calculation results[35]. Here we only focus on the configuration with the lowest total energy and, consequently, the lowest formation energy.

We start with examining the electronic characteristics via the depiction of DOS and isosurfaces of charge density

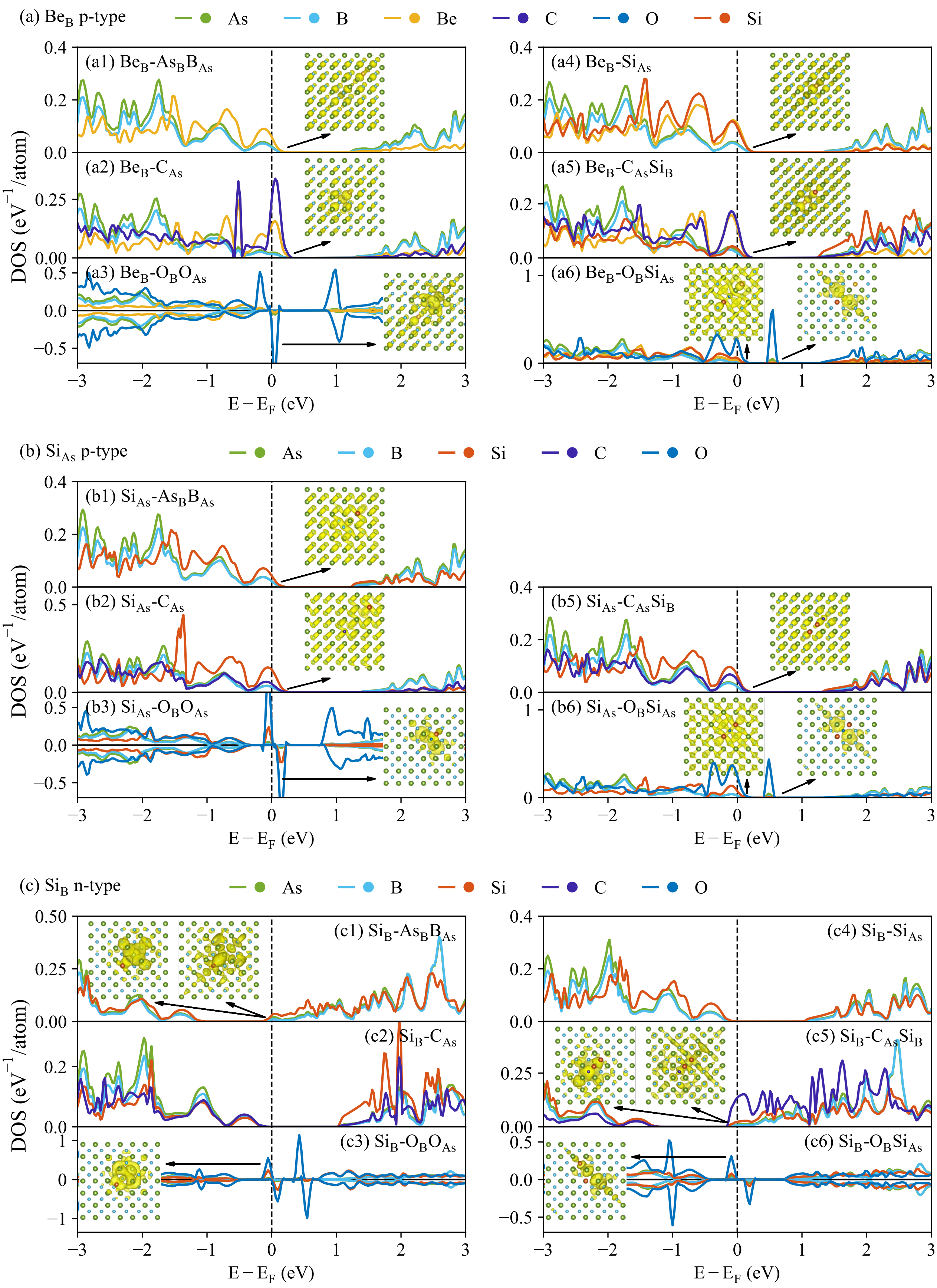

of Be_B doping (see Fig. 4(a)). As mentioned above, Be_B

and Si_{As} feature three-fold degenerated bands at VBM,

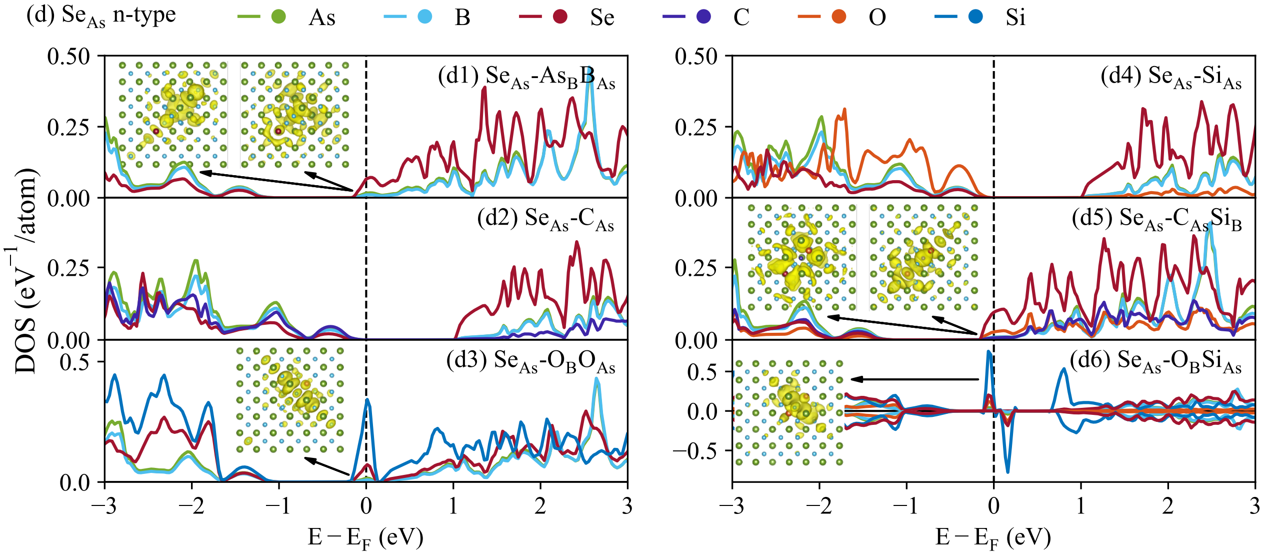

FIG. 4. Calculated electronic DOS of BAs doped by (a) Be$_B$, (b) Si$_{As}$, (c) Si$_B$, or (d) Se$_{As}$ in the presence of (1) As$_B$B$_{As}$, (2) C$_{As}$, (3) O$_B$O$_{As}$, (4) Si$_{As}$, (5) C$_{As}$Si$_B$, or (6) O$_B$Si$_{As}$ point defect. The differently colored curves represent the DOS projection on different atoms. The inset figures show the isosurfaces of charge density near VBM (<0.1 eV) or within the band gap, with the differently colored atoms representing different species.

and the presence of point defects may break the symmetry of the degenerated bands. In this case, only the highest band at VBM is shown as inset figures in Fig. 4(a) and (b), while all bands within 0.1 eV of VBM are provided in enlarged figures in Sec. V of SM[35]. Interestingly, the p-type shallow state of Be$_B$ is maintained in the presence of all six point defects. E_F is still positioned slightly below VBM, and the bands near VBM continue to exhibit spatial delocalization. This result is understandable for the charge-neutral defects As$_B$B$_{As}$ and C$_{As}$Si$_B$, as well as for the acceptor-like defects C$_{As}$ and Si$_{As}$, though the acceptor-like defects slightly shift the E_F deeper into the valence band. Surprisingly, for the donor-like defects O$_B$O$_{As}$ and O$_B$Si$_{As}$, a delocalized defect state emerges at the top of VBM, while a localized defect state is formed at the bottom of CBM (for O$_B$O$_{As}$) or within the band gap (for O$_B$Si$_{As}$). Despite the narrowed band gaps, the p-type shallow state of Be$_B$ is still maintained for both donor-like defects. For the other p-type dopant Si$_{As}$, the results are similar to those for Be$_B$; namely, As$_B$B$_{As}$, C$_{As}$, C$_{As}$Si$_B$, and O$_B$Si$_{As}$ all sustain the shallow state (see Fig. 4(b)). The only difference is that O$_B$O$_{As}$ now forms a localized trapping state in the middle of the band gap, where E_F is positioned.

Nevertheless, in the case of n-type dopants Si$_B$ and Se$_{As}$, the examined point defects exert a more significant influence, owing to the acceptor-like nature of C$_{As}$ and Si$_{As}$ impurities—for which the E_F is no longer in the conduction bands—thereby destroying the n-type nature (see Fig. 4(c) and (d))). Here, both O$_B$O$_{As}$ and O$_B$Si$_{As}$ form localized trapping states within the band gap where E_F is located. As a result, the defects that preserve the n-type shallow state are the charge-neutral defects As$_B$B$_{As}$ and C$_{As}$Si$_B$, where E_F is marginally above CBM, and one of the bands near CBM exhibits weak spatial delocalization while the other becomes predominantly localized.

Furthermore, we provide a synopsis regarding the formation energy of dopants in the presence of point defects. The bars in Fig 5 illustrate $E_f^X(D)$, the formation energy of the dopants D in the presence of each point defect X. The dashed black lines denote $E_f(D)$, the formation energy of the dopants without point defects. Green signifies that the delocalized doping state of the original type is preserved, whereas red indicates otherwise, either because the doping type is changed or the bands near E_F are localized trapping states. This color is defined by the results given in Fig. 4. Three distinct scenarios are covered: (1) a bar above the dashed line implies that the defect does not couple with the dopant, thus merely impacting the doping; (2) a red bar below the dashed line signifies that a coupled complex of the defect and dopant will likely form, potentially compromising the originally targeted doping state; (3) a green bar below the dashed line indicates that the coupled complex will likely form and preserve the shallow doping state. Only the last case is beneficial to the doping efficiency. Following these three scenarios, the O impurity proves detrimental for three types of dopants except Be$_B$, as evidenced by the results of O$_B$O$_{As}$. This necessitates restriction of O's concentration. Regarding C$_{As}$ and Si$_{As}$, for p-type dopings Be$_B$ and Si$_{As}$, concerns over C and Si impurities are alleviated; otherwise, for n-type dopings Si$_B$ and Se$_{As}$, careful removal of C and Si impurities is imperative, which again emphasizes the lower n-type

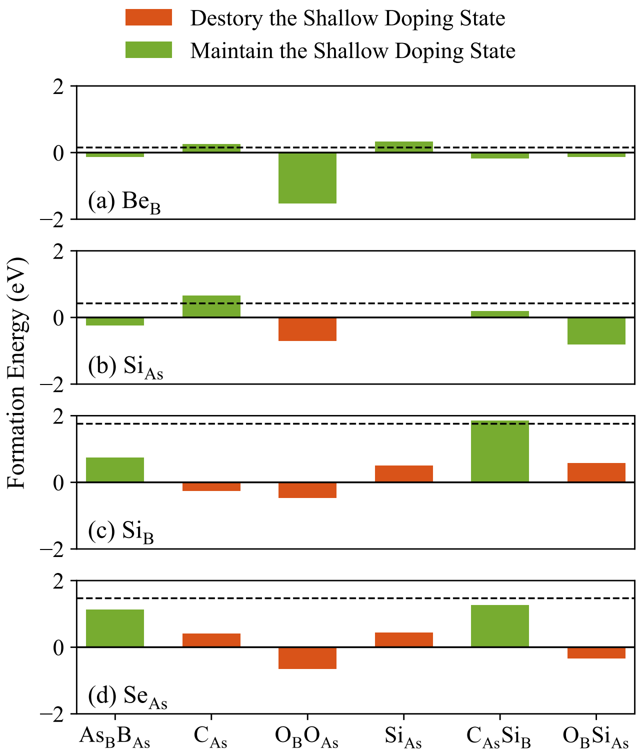

FIG. 5. Calculated formation energy of (a) Be_B, (b) Si_{As}, (c) Si_B, and (d) Se_{As} dopants in the presence of the selected point defects. The dashed lines represent the formation energy of dopants without defects.

dopability in BAs. Most interestingly, the most favorable intrinsic defect, antisite defect pair As_BB_{As}, proves beneficial for all four types of dopants. Similar results can be confirmed for the other charge-neutral defect, $C_{As}Si_B$, which also proves beneficial for three types of dopants except Si_B.

In conclusion, we have computed the formation energies and electronic characteristics of selected dopants, point defects, and coupled complexes between dopants and point defects in BAs from first principles. The shallow doping states of p-type dopants Be_B and Si_{As}, and n-type dopants Si_B and Se_{As}, were directly confirmed by the delocalized charge density isosurface near E_F. The favorable single point defects and point defect pairs for C, O, and Si impurities were identified (C_{As}, O_BO_{As}, Si_{As}, $C_{As}Si_B$, and O_BSi_{As}), all with formation energies of less than 1.5 eV. As for couplings between the selected dopants and defects, this study also identified the most favorable configurations. In terms of the influence of impurities on doping, the O impurity is detrimental to both p- and n-type doping (except Be_B), and C and Si impurities are detrimental to only n-type doping. Consequently, n-type doping is challenging, as it has a higher formation energy and requires the removal of C, Si, and O impurities. Interestingly, the most favorable intrinsic defect, antisite defect pair As_BB_{As}, positively impacts both the p- and n-type doping. These insights into the interactions between dopants and defects could potentially help expedite the advancement of advanced electronics based on BAs.

This work is supported through the INL Laboratory Directed Research and Development (LDRD) Program under DOE Idaho Operations Office Contract DE-AC07-05ID14517, LDRD Project ID 23A1070-064FP. This research made use of Idaho National Laboratory's High Performance Computing systems located at the Collaborative Computing Center and supported by the Office of Nuclear Energy of the U.S. Department of Energy and the Nuclear Science User Facilities under Contract No. DE-AC07-05ID14517.

[1] D. A. Broido, L. Lindsay, and T. L. Reinecke, Physical Review B **88**, 214303 (2013).
[2] L. Lindsay, D. A. Broido, and T. L. Reinecke, Physical Review Letters **111**, 025901 (2013).
[3] T. Feng, L. Lindsay, and X. Ruan, Physical Review B **96**, 161201 (2017).
[4] J. S. Kang, M. Li, H. Wu, H. Nguyen, and Y. Hu, Science **361**, 575 (2018).
[5] F. Tian, B. Song, X. Chen, N. K. Ravichandran, Y. Lv, K. Chen, S. Sullivan, J. Kim, Y. Zhou, T.-H. Liu, M. Goni, Z. Ding, J. Sun, G. A. G. Udalamatta Gamage, H. Sun, H. Ziyaee, S. Huyan, L. Deng, J. Zhou, A. J. Schmidt, S. Chen, C.-W. Chu, P. Y. Huang, D. Broido, L. Shi, G. Chen, and Z. Ren, Science **361**, 582 (2018).
[6] S. Li, Q. Zheng, Y. Lv, X. Liu, X. Wang, P. Y. Huang, D. G. Cahill, and B. Lv, Science **361**, 579 (2018).
[7] T.-H. Liu, B. Song, L. Meroueh, Z. Ding, Q. Song, J. Zhou, M. Li, and G. Chen, Physical Review B **98**, 081203 (2018).
[8] J. Shin, G. A. Gamage, Z. Ding, K. Chen, F. Tian, X. Qian, J. Zhou, H. Lee, J. Zhou, L. Shi, T. Nguyen, F. Han, M. Li, D. Broido, A. Schmidt, Z. Ren, and G. Chen, Science **377**, 437 (2022).
[9] S. Yue, F. Tian, X. Sui, M. Mohebinia, X. Wu, T. Tong, Z. Wang, B. Wu, Q. Zhang, Z. Ren, J. Bao, and X. Liu, Science **377**, 433 (2022).
[10] G. L. W. Hart and A. Zunger, Physical Review B **62**, 13522 (2000).
[11] R. M. Wentzcovitch and M. L. Cohen, Journal of Physics C: Solid State Physics **19**, 6791 (1986).
[12] T. Joshi, P. Kumar, B. Poudyal, S. P. Russell, P. Manchanda, and P. Dev, Physical Review B **105**, 054101 (2022).
[13] J. Xing, E. R. Glaser, B. Song, J. C. Culbertson, J. A. Freitas, Jr., R. A. Duncan, K. A. Nelson, G. Chen, and N. Ni, Applied Physics Letters **112**, 241903 (2018).
[14] F. Tian, B. Song, B. Lv, J. Sun, S. Huyan, Q. Wu, J. Mao, Y. Ni, Z. Ding, S. Huberman, T.-H. Liu, G. Chen, S. Chen, C.-W. Chu, and Z. Ren, Applied Physics Letters **112**, 031903 (2018).
[15] G. A. Gamage, H. Sun, H. Ziyaee, F. Tian, and Z. Ren, Applied Physics Letters **115**, 092103 (2019).
[16] G. A. Gamage, K. Chen, G. Chen, F. Tian, and Z. Ren, Materials Today Physics **11**, 100160 (2019).
[17] B. Lv, Y. Lan, X. Wang, Q. Zhang, Y. Hu, A. J. Jacobson, D. Broido, G. Chen, Z. Ren, and C.-W. Chu, Applied Physics Letters **106**, 074105 (2015).
[18] J. Kim, D. A. Evans, D. P. Sellan, O. M. Williams, E. Ou, A. H. Cowley, and L. Shi, Applied Physics Letters **108**, 201905 (2016).
[19] J. Xing, X. Chen, Y. Zhou, James. C. Culbertson, J. A. Freitas, Jr., E. R. Glaser, J. Zhou, L. Shi, and N. Ni, Applied Physics Letters **112**, 261901 (2018).
[20] T. L. Chu and A. E. Hyslop, Journal of Applied Physics **43**, 276 (2003).
[21] Q. Zheng, C. A. Polanco, M.-H. Du, L. R. Lindsay, M. Chi,

J. Yan, and B. C. Sales, Physical Review Letters **121**, 105901 (2018).

[22] N. H. Protik, J. Carrete, N. A. Katcho, N. Mingo, and D. Broido, Physical Review B **94**, 045207 (2016).

[23] M. Fava, N. H. Protik, C. Li, N. K. Ravichandran, J. Carrete, A. van Roekeghem, G. K. H. Madsen, N. Mingo, and D. Broido, npj Computational Materials **7**, 1 (2021).

[24] X. Chen, C. Li, Y. Xu, A. Dolocan, G. Seward, A. Van Roekeghem, F. Tian, J. Xing, S. Guo, N. Ni, Z. Ren, J. Zhou, N. Mingo, D. Broido, and L. Shi, Chemistry of Materials **33**, 6974 (2021).

[25] J. Tang, G. Li, Q. Wang, J. Zheng, L. Cheng, and R. Guo, Physical Review Materials **7**, 044601 (2023).

[26] S. Chae, K. Mengle, J. T. Heron, and E. Kioupakis, Applied Physics Letters **113**, 212101 (2018).

[27] J. L. Lyons, J. B. Varley, E. R. Glaser, J. A. Freitas, Jr., J. C. Culbertson, F. Tian, G. A. Gamage, H. Sun, H. Ziyaee, and Z. Ren, Applied Physics Letters **113**, 251902 (2018).

[28] K. Bushick, K. Mengle, N. Sanders, and E. Kioupakis, Applied Physics Letters **114**, 022101 (2019).

[29] P. E. Blöchl, Physical Review B **50**, 17953 (1994).

[30] G. Kresse and D. Joubert, Physical Review B **59**, 1758 (1999).

[31] G. Kresse and J. Hafner, Physical Review B **47**, 558 (1993).

[32] G. Kresse and J. Furthmüller, Physical Review B **54**, 11169 (1996).

[33] J. P. Perdew, A. Ruzsinszky, G. I. Csonka, O. A. Vydrov, G. E. Scuseria, L. A. Constantin, X. Zhou, and K. Burke, Physical Review Letters **100**, 136406 (2008).

[34] J. Heyd, G. E. Scuseria, and M. Ernzerhof, The Journal of Chemical Physics **118**, 8207 (2003).

[35] See Supplemental Materials at [link] for information about formation energy of charged intrinsic defects in cubic BAs, BP, and BN, formation energy of charged dopants in BAs, calculated configurations of coupled dopants and point defects, calculated DOS and formation energy for extra defects besides the ones presented in the main text, and enlarged figures of isosurfaces of charge density. See also Refs.[37,38].

[36] K. Momma and F. Izumi, Journal of Applied Crystallography **44**, 1272 (2011).

[37] C. Freysoldt, J. Neugebauer, and C. G. Van de Walle, Physical Review Letters **102**, 016402 (2009).

[38] J. Buckeridge and D. O. Scanlon, Physical Review Materials **3**, 051601 (2019).

arXiv:2403.09013v1 [cond-mat.mtrl-sci] 14 Mar 2024

Supplemental materials to

Impacts of Point Defects on Shallow Doping in Cubic Boron Arsenide: A First Principles Study

Shuxiang Zhou[1], Zilong Hua[1], Kaustubh K. Bawane[1], Hao Zhou[2], and Tianli Feng[2]
[1] *Idaho National Laboratory, Idaho Falls, Idaho 83415, USA*
[2] *Department of Mechanical Engineering, University of Utah, Salt Lake City, Utah 84112, USA*

I. FORMATION ENERGY OF DOPANTS WITH THE PRESENCE OF POINT DEFECTS

The formation energy E_f of a defect (or a dopant) X in pristine BAs is calculated by:

$$E_f(X) = E(X) - E_0 - \sum_i n_i^X (E_i + \mu_i) \tag{S1}$$

where E_0 is the total energy of pristine system, $E(X)$ is the total energy of the defected system, n_i^X represents the number of atoms of species i changed according to the defect X (positive if atoms are added, negatives if atoms are removed), E_i is the energy per atom in the elemental phase, and μ_i is the chemical potential of species i. Therefore, the formation energy of a coupled complex of dopant and defect D-X is calculated by:

$$E_f(D\text{-}X) = E(D\text{-}X) - E_0 - \sum_i n_i^{D\text{-}X} (E_i + \mu_i) = E(D\text{-}X) - E_0 - \sum_i n_i^D (E_i + \mu_i) - \sum_i n_i^X (E_i + \mu_i) \tag{S2}$$

As for the formation energy of a dopant D in presence of a defect X, the reference state is the defected BAs rather than pristine BAs:

$$E_f^X(D) = E(D\text{-}X) - E(X) - \sum_i n_i^D (E_i + \mu_i) \tag{S3}$$

By combining Eq. S1-S3, one can obtain

$$E_f^X(D) = E_f(D\text{-}X) - E_f(X) \tag{S4}$$

II. FORMATION ENERGY CALCULATION OF DOPANTS IN BAs

The formation energy of charged p-type dopants ($\mathrm{Be_B}$, $\mathrm{C_{As}}$, $\mathrm{Si_{As}}$, and $\mathrm{Ge_{As}}$) and n-type dopants ($\mathrm{Se_{As}}$, $\mathrm{C_B}$, $\mathrm{Si_B}$, and $\mathrm{Ge_B}$) as a function of the Fermi level E_F was computed using PBEsol (see Fig. S1). For a dopant D with charge q, the formation energy $E_f(D^q)$ given by):

$$E_f(D^q) = E(D^q) - E_0 - \sum_i n_i^D(E_i + \mu_i) + q(E_F + E_{VBM}) + E_{corr}(D^q) \tag{S5}$$

The formation energy of a charged dopant depends on the Fermi level E_F, which is referenced to the energy of the valence band maximum (VBM), E_{VBM}. Specifically, E_F spans from zero to the band gap E_{gap}, wherein $E_F = 0$ signifies the Fermi level resting on the VBM, and $E_F = E_{gap}$ indicates that the Fermi level aligns with the conduction band minimum (CBM). In DFT calculations involving non-zero charges, it becomes necessary to simulate a neutralizing background to circumvent infinite charge issues under periodic boundary conditions. Thereby, a correction energy E_{corr} is introduced to account for the nonphysical electrostatic interaction between periodic charged-defect images, which is computed using SXDEFECTALIGN package [1]. The charges q computed in the systems varied from -2 to 2.

Comparing with the HSE results from Ref. [2–4], beside the underpredicted band gap, the ionization energy is overpredicted in our PBEsol calculations. However, the formation energy is comparable between our PBEsol results and previous HSE results, where $\mathrm{Be_B}$ and $\mathrm{Si_{As}}$ are the two p-type dopants with the lowest formation energy, while $\mathrm{Se_{As}}$ and $\mathrm{Si_B}$ are the two n-type dopants with the lowest formation energy.

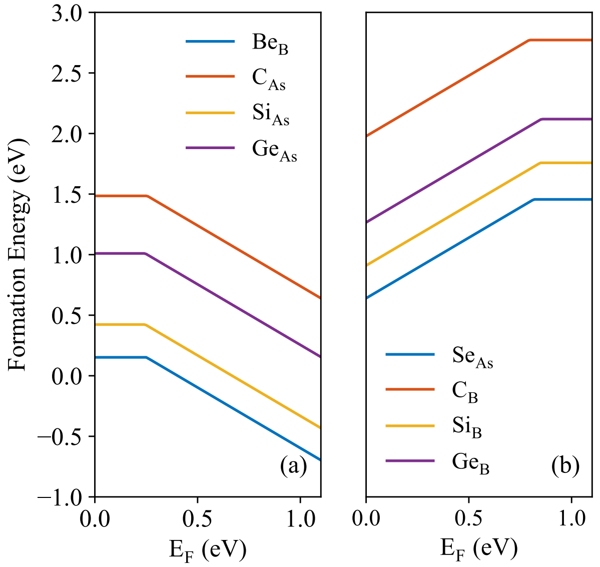

FIG. S1. Calculated formation energies of (a) p-type dopants and (b) n-type dopants, as function of Fermi energy, which the minimum and maximum values are corresponding to VBM and CBM, respectively.

III. CONFIGURATIONS OF COUPLED COMPLEX OF DOPANTS AND POINT DEFECTS

For each coupled complex of dopants and point defects, we compute multiple configurations, where the dopants and point defects occupy different sites. We first tabulate the the fractional coordinates of each site (see Table S1), then provide the total energy of each configuration (see Table S2-S7). For each coupled complex, the lowest total energy is highlighted in bold text, to indicate the specific configuration used in the DOS and formation energy calculation. The dopants include $\mathrm{Be_B}$, $\mathrm{Si_{As}}$, $\mathrm{Se_{As}}$, and $\mathrm{Si_B}$, and the point defects include $\mathrm{C_{As}}$, $\mathrm{O_BO_{As}}$, $\mathrm{Si_{As}}$, $\mathrm{C_{As}Si_B}$, $\mathrm{O_BSi_{As}}$, $\mathrm{As_BB_{As}}$ (as discussed in the main text), $\mathrm{As_B}$, $\mathrm{B_{As}}$, and $\mathrm{N_{As}}$ (as discussed in the following section). Therefore, the coupled complexes can be categorized into six groups:

- $\mathrm{D_B}$-$\mathrm{X_{As}}$, where D = Be or Si, X = C, Si, B, or N
- $\mathrm{D_{As}}$-$\mathrm{X_{As}}$, where D = Si or Se, X = C, Si, B, or N, excluding that both D and X = Si;
- $\mathrm{D_B}$-$\mathrm{X_BY_{As}}$, where D = Be or Si, (X, Y) = (O, O), (Si, C), (O, Si), or (As, B);
- $\mathrm{D_{As}}$-$\mathrm{X_BY_{As}}$, where D = Si or Se, (X, Y) = (O, O), (Si, C), (O, Si), or (As, B);
- $\mathrm{D_B}$-$\mathrm{X_B}$, where D = Be or Si, X = As;
- $\mathrm{D_{As}}$-$\mathrm{X_B}$, where D = Si or Se, X = As.

TABLE S1: The fractional coordinates of each B and As sites in the $3 \times 3 \times 3$ supercell of the conventional cubic cell of BAs.

Sites	Fractional coordinates	Sites	Fractional coordinates	Sites	Fractional coordinates	Sites	Fractional coordinates
As1	(0, 0, 0)	As55	(0.5, 0, 0.1667)	B1	(0.0833, 0.0833, 0.0833)	B55	(0.5833, 0.0833, 0.25)
As2	(0, 0, 0.3333)	As56	(0.5, 0, 0.5)	B2	(0.0833, 0.0833, 0.4167)	B56	(0.5833, 0.0833, 0.5833)
As3	(0, 0, 0.6667)	As57	(0.5, 0, 0.8333)	B3	(0.0833, 0.0833, 0.75)	B57	(0.5833, 0.0833, 0.9167)
As4	(0, 0.1667, 0.1667)	As58	(0.5, 0.1667, 0)	B4	(0.0833, 0.25, 0.25)	B58	(0.5833, 0.25, 0.0833)
As5	(0, 0.1667, 0.5)	As59	(0.5, 0.1667, 0.3333)	B5	(0.0833, 0.25, 0.5833)	B59	(0.5833, 0.25, 0.4167)
As6	(0, 0.1667, 0.8333)	As60	(0.5, 0.1667, 0.6667)	B6	(0.0833, 0.25, 0.9167)	B60	(0.5833, 0.25, 0.75)
As7	(0, 0.3333, 0)	As61	(0.5, 0.3333, 0.1667)	B7	(0.0833, 0.4167, 0.0833)	B61	(0.5833, 0.4167, 0.25)
As8	(0, 0.3333, 0.3333)	As62	(0.5, 0.3333, 0.5)	B8	(0.0833, 0.4167, 0.4167)	B62	(0.5833, 0.4167, 0.5833)
As9	(0, 0.3333, 0.6667)	As63	(0.5, 0.3333, 0.8333)	B9	(0.0833, 0.4167, 0.75)	B63	(0.5833, 0.4167, 0.9167)
As10	(0, 0.5, 0.1667)	As64	(0.5, 0.5, 0)	B10	(0.0833, 0.5833, 0.25)	B64	(0.5833, 0.5833, 0.0833)
As11	(0, 0.5, 0.5)	As65	(0.5, 0.5, 0.3333)	B11	(0.0833, 0.5833, 0.5833)	B65	(0.5833, 0.5833, 0.4167)
As12	(0, 0.5, 0.8333)	As66	(0.5, 0.5, 0.6667)	B12	(0.0833, 0.5833, 0.9167)	B66	(0.5833, 0.5833, 0.75)
As13	(0, 0.6667, 0)	As67	(0.5, 0.6667, 0.1667)	B13	(0.0833, 0.75, 0.0833)	B67	(0.5833, 0.75, 0.25)
As14	(0, 0.6667, 0.3333)	As68	(0.5, 0.6667, 0.5)	B14	(0.0833, 0.75, 0.4167)	B68	(0.5833, 0.75, 0.5833)
As15	(0, 0.6667, 0.6667)	As69	(0.5, 0.6667, 0.8333)	B15	(0.0833, 0.75, 0.75)	B69	(0.5833, 0.75, 0.9167)
As16	(0, 0.8333, 0.1667)	As70	(0.5, 0.8333, 0)	B16	(0.0833, 0.9167, 0.25)	B70	(0.5833, 0.9167, 0.0833)
As17	(0, 0.8333, 0.5)	As71	(0.5, 0.8333, 0.3333)	B17	(0.0833, 0.9167, 0.5833)	B71	(0.5833, 0.9167, 0.4167)
As18	(0, 0.8333, 0.8333)	As72	(0.5, 0.8333, 0.6667)	B18	(0.0833, 0.9167, 0.9167)	B72	(0.5833, 0.9167, 0.75)
As19	(0.1667, 0, 0.1667)	As73	(0.6667, 0, 0)	B19	(0.25, 0.0833, 0.25)	B73	(0.75, 0.0833, 0.0833)
As20	(0.1667, 0, 0.5)	As74	(0.6667, 0, 0.3333)	B20	(0.25, 0.0833, 0.5833)	B74	(0.75, 0.0833, 0.4167)
As21	(0.1667, 0, 0.8333)	As75	(0.6667, 0, 0.6667)	B21	(0.25, 0.0833, 0.9167)	B75	(0.75, 0.0833, 0.75)
As22	(0.1667, 0.1667, 0)	As76	(0.6667, 0.1667, 0.1667)	B22	(0.25, 0.25, 0.0833)	B76	(0.75, 0.25, 0.25)
As23	(0.1667, 0.1667, 0.3333)	As77	(0.6667, 0.1667, 0.5)	B23	(0.25, 0.25, 0.4167)	B77	(0.75, 0.25, 0.5833)
As24	(0.1667, 0.1667, 0.6667)	As78	(0.6667, 0.1667, 0.8333)	B24	(0.25, 0.25, 0.75)	B78	(0.75, 0.25, 0.9167)
As25	(0.1667, 0.3333, 0.1667)	As79	(0.6667, 0.3333, 0)	B25	(0.25, 0.4167, 0.25)	B79	(0.75, 0.4167, 0.0833)
As26	(0.1667, 0.3333, 0.5)	As80	(0.6667, 0.3333, 0.3333)	B26	(0.25, 0.4167, 0.5833)	B80	(0.75, 0.4167, 0.4167)
As27	(0.1667, 0.3333, 0.8333)	As81	(0.6667, 0.3333, 0.6667)	B27	(0.25, 0.4167, 0.9167)	B81	(0.75, 0.4167, 0.75)
As28	(0.1667, 0.5, 0)	As82	(0.6667, 0.5, 0.1667)	B28	(0.25, 0.5833, 0.0833)	B82	(0.75, 0.5833, 0.25)
As29	(0.1667, 0.5, 0.3333)	As83	(0.6667, 0.5, 0.5)	B29	(0.25, 0.5833, 0.4167)	B83	(0.75, 0.5833, 0.5833)
As30	(0.1667, 0.5, 0.6667)	As84	(0.6667, 0.5, 0.8333)	B30	(0.25, 0.5833, 0.75)	B84	(0.75, 0.5833, 0.9167)
As31	(0.1667, 0.6667, 0.1667)	As85	(0.6667, 0.6667, 0)	B31	(0.25, 0.75, 0.25)	B85	(0.75, 0.75, 0.0833)
As32	(0.1667, 0.6667, 0.5)	As86	(0.6667, 0.6667, 0.3333)	B32	(0.25, 0.75, 0.5833)	B86	(0.75, 0.75, 0.4167)
As33	(0.1667, 0.6667, 0.8333)	As87	(0.6667, 0.6667, 0.6667)	B33	(0.25, 0.75, 0.9167)	B87	(0.75, 0.75, 0.75)
As34	(0.1667, 0.8333, 0)	As88	(0.6667, 0.8333, 0.1667)	B34	(0.25, 0.9167, 0.0833)	B88	(0.75, 0.9167, 0.25)
As35	(0.1667, 0.8333, 0.3333)	As89	(0.6667, 0.8333, 0.5)	B35	(0.25, 0.9167, 0.4167)	B89	(0.75, 0.9167, 0.5833)
As36	(0.1667, 0.8333, 0.6667)	As90	(0.6667, 0.8333, 0.8333)	B36	(0.25, 0.9167, 0.75)	B90	(0.75, 0.9167, 0.9167)

TABLE S1: The fractional coordinates of each B and As sites in the $3 \times 3 \times 3$ supercell of the conventional cubic cell of BAs.

Sites	Fractional coordinates	Sites	Fractional coordinates	Sites	Fractional coordinates	Sites	Fractional coordinates
As37	(0.3333, 0, 0)	As91	(0.8333, 0, 0.1667)	B37	(0.4167, 0.0833, 0.0833)	B91	(0.9167, 0.0833, 0.25)
As38	(0.3333, 0, 0.3333)	As92	(0.8333, 0, 0.5)	B38	(0.4167, 0.0833, 0.4167)	B92	(0.9167, 0.0833, 0.5833)
As39	(0.3333, 0, 0.6667)	As93	(0.8333, 0, 0.8333)	B39	(0.4167, 0.0833, 0.75)	B93	(0.9167, 0.0833, 0.9167)
As40	(0.3333, 0.1667, 0.1667)	As94	(0.8333, 0.1667, 0)	B40	(0.4167, 0.25, 0.25)	B94	(0.9167, 0.25, 0.0833)
As41	(0.3333, 0.1667, 0.5)	As95	(0.8333, 0.1667, 0.3333)	B41	(0.4167, 0.25, 0.5833)	B95	(0.9167, 0.25, 0.4167)
As42	(0.3333, 0.1667, 0.8333)	As96	(0.8333, 0.1667, 0.6667)	B42	(0.4167, 0.25, 0.9167)	B96	(0.9167, 0.25, 0.75)
As43	(0.3333, 0.3333, 0)	As97	(0.8333, 0.3333, 0.1667)	B43	(0.4167, 0.4167, 0.0833)	B97	(0.9167, 0.4167, 0.25)
As44	(0.3333, 0.3333, 0.3333)	As98	(0.8333, 0.3333, 0.5)	B44	(0.4167, 0.4167, 0.4167)	B98	(0.9167, 0.4167, 0.5833)
As45	(0.3333, 0.3333, 0.6667)	As99	(0.8333, 0.3333, 0.8333)	B45	(0.4167, 0.4167, 0.75)	B99	(0.9167, 0.4167, 0.9167)
As46	(0.3333, 0.5, 0.1667)	As100	(0.8333, 0.5, 0)	B46	(0.4167, 0.5833, 0.25)	B100	(0.9167, 0.5833, 0.0833)
As47	(0.3333, 0.5, 0.5)	As101	(0.8333, 0.5, 0.3333)	B47	(0.4167, 0.5833, 0.5833)	B101	(0.9167, 0.5833, 0.4167)
As48	(0.3333, 0.5, 0.8333)	As102	(0.8333, 0.5, 0.6667)	B48	(0.4167, 0.5833, 0.9167)	B102	(0.9167, 0.5833, 0.75)
As49	(0.3333, 0.6667, 0)	As103	(0.8333, 0.6667, 0.1667)	B49	(0.4167, 0.75, 0.0833)	B103	(0.9167, 0.75, 0.25)
As50	(0.3333, 0.6667, 0.3333)	As104	(0.8333, 0.6667, 0.5)	B50	(0.4167, 0.75, 0.4167)	B104	(0.9167, 0.75, 0.5833)
As51	(0.3333, 0.6667, 0.6667)	As105	(0.8333, 0.6667, 0.8333)	B51	(0.4167, 0.75, 0.75)	B105	(0.9167, 0.75, 0.9167)
As52	(0.3333, 0.8333, 0.1667)	As106	(0.8333, 0.8333, 0)	B52	(0.4167, 0.9167, 0.25)	B106	(0.9167, 0.9167, 0.0833)
As53	(0.3333, 0.8333, 0.5)	As107	(0.8333, 0.8333, 0.3333)	B53	(0.4167, 0.9167, 0.5833)	B107	(0.9167, 0.9167, 0.4167)
As54	(0.3333, 0.8333, 0.8333)	As108	(0.8333, 0.8333, 0.6667)	B54	(0.4167, 0.9167, 0.9167)	B108	(0.9167, 0.9167, 0.75)

TABLE S2. For the coupled complex of dopant and defect $\mathrm{D_B}$-$\mathrm{X_{As}}$, where D = Be or Si, X = C, Si, B, or N, the total energy $E(\mathrm{D_B}$-$\mathrm{X_{As}})$ and the distance d between $\mathrm{D_B}$ and $\mathrm{X_{As}}$ as functions of the site of $\mathrm{D_B}$. The site of $\mathrm{X_{As}}$ is at As1.

Site of $\mathrm{D_B}$	d (Å)	$E(\mathrm{Be_B}$-$\mathrm{C_{As}})$ (eV)	$E(\mathrm{Be_B}$-$\mathrm{Si_{As}})$ (eV)	$E(\mathrm{Be_B}$-$\mathrm{B_{As}})$ (eV)	$E(\mathrm{Be_B}$-$\mathrm{N_{As}})$ (eV)	$E(\mathrm{Si_B}$-$\mathrm{C_{As}})$ (eV)	$E(\mathrm{Si_B}$-$\mathrm{Si_{As}})$ (eV)	$E(\mathrm{Si_B}$-$\mathrm{B_{As}})$ (eV)	$E(\mathrm{Si_B}$-$\mathrm{N_{As}})$ (eV)
B1	2.07	**-1317.62**	-1314.11	**-1314.81**	**-1318.44**	**-1319.89**	**-1316.28**	**-1317.07**	**-1318.34**
B21	3.96	-1317.33	-1314.60	-1313.99	-1317.18	-1318.77	-1315.97	-1315.70	-1317.40
B22	5.21	-1317.54	-1314.62	-1314.22	-1317.39	-1318.84	-1315.92	-1315.68	-1317.57
B2	6.21	-1317.47	**-1314.69**	-1314.14	-1317.25	-1318.70	-1315.87	-1315.53	-1317.44

TABLE S3. For the coupled complex of dopant and defect $\mathrm{D_{As}}$-$\mathrm{X_{As}}$, where D = Si or Se, X = C, Si, B, or N, the total energy $E(\mathrm{D_{As}}$-$\mathrm{X_{As}})$ and the distance d between $\mathrm{D_{As}}$ and $\mathrm{X_{As}}$ as functions of the site of $\mathrm{D_{As}}$. The site of $\mathrm{X_{As}}$ is at As1.

Site of $\mathrm{D_{As}}$	d (Å)	$E(\mathrm{Si_{As}}$-$\mathrm{C_{As}})$ (eV)	$E(\mathrm{Si_{As}}$-$\mathrm{B_{As}})$ (eV)	$E(\mathrm{Si_{As}}$-$\mathrm{N_{As}})$ (eV)	$E(\mathrm{Se_{As}}$-$\mathrm{C_{As}})$ (eV)	$E(\mathrm{Se_{As}}$-$\mathrm{Si_{As}})$ (eV)	$E(\mathrm{Se_{As}}$-$\mathrm{B_{As}})$ (eV)	$E(\mathrm{Se_{As}}$-$\mathrm{N_{As}})$ (eV)
As21	3.38	-1320.74	-1317.49	-1320.72	**-1319.26**	**-1316.38**	**-1316.23**	**-1317.82**
As2	4.78	-1320.90	-1317.56	-1320.72	-1319.07	-1316.24	-1315.93	-1317.78
As23	5.85	-1320.93	-1317.54	-1320.72	-1319.03	-1316.21	-1315.87	-1317.77
As38	6.76	**-1320.96**	**-1317.58**	**-1320.74**	-1319.00	-1316.20	-1315.83	-1317.75

TABLE S4. For the coupled complex of dopant and defect $\mathrm{D_B}$-$\mathrm{X_B Y_{As}}$, where D = Be or Si, (X, Y) = (O, O), (Si, C), (O, Si), or (As, B), the total energy $E(\mathrm{D_B}$-$\mathrm{X_B Y_{As}})$, the distance d_1 between $\mathrm{D_B}$ and $\mathrm{X_B}$, and the distance d_2 between $\mathrm{D_B}$ and $\mathrm{Y_{As}}$, as functions of the site of $\mathrm{D_B}$. The sites of $\mathrm{X_B}$ and $\mathrm{Y_{As}}$ are at B1 and As1, respectively.

Site of $\mathrm{D_B}$	d_1 (Å)	d_2 (Å)	$E(\mathrm{Be_B}$-$\mathrm{O_B O_{As}})$ (eV)	$E(\mathrm{Be_B}$-$\mathrm{Si_B C_{As}})$ (eV)	$E(\mathrm{Be_B}$-$\mathrm{O_B Si_{As}})$ (eV)	$E(\mathrm{Be_B}$-$\mathrm{As_B B_{As}})$ (eV)	$E(\mathrm{Si_B}$-$\mathrm{O_B O_{As}})$ (eV)	$E(\mathrm{Si_B}$-$\mathrm{Si_B C_{As}})$ (eV)	$E(\mathrm{Si_B}$-$\mathrm{O_B Si_{As}})$ (eV)	$E(\mathrm{Si_B}$-$\mathrm{As_B B_{As}})$ (eV)
B106	3.38	2.07	**-1315.45**	**-1316.95**	-1312.81	-1312.29	**-1316.14**	**-1316.68**	-1314.12	**-1313.84**
B94	3.38	3.96	-1314.11	-1316.66	-1313.34	-1312.81	-1314.40	-1316.02	**-1314.63**	-1312.81
B3	4.78	3.96	-1313.77	-1316.52	-1313.21	-1312.57	-1313.83	-1316.12	-1313.98	-1312.99
B4	3.38	5.21	-1313.87	-1316.83	**-1313.58**	**-1312.96**	-1314.37	-1315.99	-1314.19	-1312.70
B108	5.85	3.96	-1313.74	-1316.50	-1313.18	-1312.54	-1313.80	-1316.13	-1314.18	-1313.02
B88	5.85	5.21	-1314.05	-1316.70	-1313.24	-1312.69	-1314.19	-1316.12	-1314.23	-1313.03
B2	4.78	6.21	-1313.85	-1316.67	-1313.24	-1312.78	-1313.92	-1316.04	-1314.17	-1312.85

TABLE S5. For the coupled complex of dopant and defect $\mathrm{D_{As}}$-$\mathrm{X_B Y_{As}}$, where D = Si or Se, (X, Y) = (O, O), (Si, C), (O, Si), or (As, B), the total energy $E(\mathrm{D_{As}}$-$\mathrm{X_B Y_{As}})$, the distance d_1 between $\mathrm{D_{As}}$ and $\mathrm{X_B}$, and the distance d_2 between $\mathrm{D_{As}}$ and $\mathrm{Y_{As}}$, as functions of the site of $\mathrm{D_{As}}$. The sites of $\mathrm{X_B}$ and $\mathrm{Y_{As}}$ are at B1 and As1, respectively.

Site of $\mathrm{D_{As}}$	d_1 (Å)	d_2 (Å)	$E(\mathrm{Si_{As}}$-$\mathrm{O_B O_{As}})$ (eV)	$E(\mathrm{Si_{As}}$-$\mathrm{Si_B C_{As}})$ (eV)	$E(\mathrm{Si_{As}}$-$\mathrm{O_B Si_{As}})$ (eV)	$E(\mathrm{Si_{As}}$-$\mathrm{As_B B_{As}})$ (eV)	$E(\mathrm{Se_{As}}$-$\mathrm{O_B O_{As}})$ (eV)	$E(\mathrm{Se_{As}}$-$\mathrm{Si_B C_{As}})$ (eV)	$E(\mathrm{Se_{As}}$-$\mathrm{O_B Si_{As}})$ (eV)	$E(\mathrm{Se_{As}}$-$\mathrm{As_B B_{As}})$ (eV)
As19	2.07	3.38	**-1318.36**	**-1320.33**	**-1318.00**	**-1316.81**	**-1315.76**	-1317.08	**-1315.58**	-1313.28
As21	3.96	3.38	-1317.40	-1319.18	-1316.66	-1316.00	-1314.40	-1317.26	-1314.67	-1313.42
As2	3.96	4.78	-1317.37	-1319.35	-1316.72	-1316.27	-1314.25	-1317.09	-1314.59	-1313.16
As93	5.21	3.38	-1317.28	-1319.29	-1316.65	-1315.96	-1314.28	**-1317.31**	-1314.34	**-1313.50**
As23	3.96	5.85	-1317.36	-1319.39	-1316.76	-1316.35	-1314.24	-1317.05	-1314.55	-1313.10
As3	6.21	4.78	-1317.29	-1319.29	-1316.70	-1316.10	-1314.22	-1317.17	-1314.21	-1313.30
As42	5.21	5.85	-1317.42	-1319.47	-1316.83	-1316.25	-1314.46	-1317.13	-1314.59	-1313.21

TABLE S6. For the coupled complex of dopant and defect D_B-As_B, where D = Be or Si, the total energy $E(D_B\text{-}As_B)$ and the distance d between D_B and As_B as functions of the site of D_B. The site of As_B is at B1.

Site of D_B	d (Å)	$E(Be_B\text{-}As_B)$ (eV)	$E(Si_B\text{-}As_B)$ (eV)
B22	3.38	**-1310.16**	-1309.24
B2	4.78	-1309.97	-1309.36
B23	5.85	-1309.95	**-1309.37**
B38	6.76	-1309.88	-1309.29

TABLE S7. For the coupled complex of dopant and defect D_{As}-As_B, where D = Si or Se, the total energy $E(D_{As}\text{-}As_B)$ and the distance d between D_{As} and As_B as functions of the site of D_{As}. The site of As_B is at B1.

Site of D_{As}	d (Å)	$E(Si_{As}\text{-}As_B)$ (eV)	$E(Se_{As}\text{-}As_B)$ (eV)
As1	2.07	**-1314.18**	**-1310.50**
As2	3.96	-1313.54	-1309.64
As38	5.21	-1313.50	-1309.73
As44	6.21	-1313.38	-1309.69

IV. INFLUENCE OF OTHER DEFECTS ON THE DOPANTS

In this section we present the results for defects $\mathrm{As_B}$, $\mathrm{B_{As}}$, and $\mathrm{N_{As}}$. $\mathrm{As_B}$ and $\mathrm{B_{As}}$ are common antisite defects, while $\mathrm{N_{As}}$ is an charge-neutral impurity, as N is in the same group of As. In N single point defects and the point defect pairs in the first nearest neighbors, the formation energies per point defect are 2.56, 0.82, 0.90, 2.59, 1.00 eV for $\mathrm{N_B}$, $\mathrm{N_{As}}$, $\mathrm{N_BN_{As}}$, $\mathrm{N_BN_B}$, and $\mathrm{N_{As}N_{As}}$, respectively. Therefore, $\mathrm{N_{As}}$ is the most favorable among these defects. The DOS and isosurface results are presented in Fig. S2-S5, and the formation energy is in Fig. S6. $\mathrm{As_B}$ is harmful to p-type dopants, and is beneficial to $\mathrm{Se_{As}}$; $\mathrm{B_{As}}$ is harmful to n-type dopants, and is beneficial to $\mathrm{Be_B}$. While $\mathrm{N_{As}}$ does not couple with As-site dopants $\mathrm{Si_{As}}$ and $\mathrm{Se_{As}}$, it is beneficial to $\mathrm{Be_B}$, as a p-type B-site dopant, and is harmful to $\mathrm{Si_B}$, as a n-type B-site dopant.

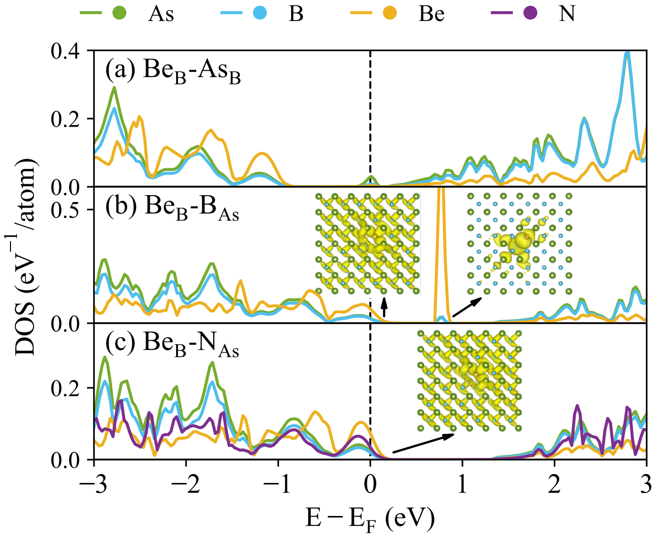

FIG. S2. Calculated electronic DOS of $\mathrm{Be_B}$-doped BAs in the presence of (a) $\mathrm{As_B}$, (b) $\mathrm{B_{As}}$, and (c) $\mathrm{N_{As}}$ point defect. The inset figures show the isosurfaces of charge density near VBM (<0.1eV) or within the band gap.

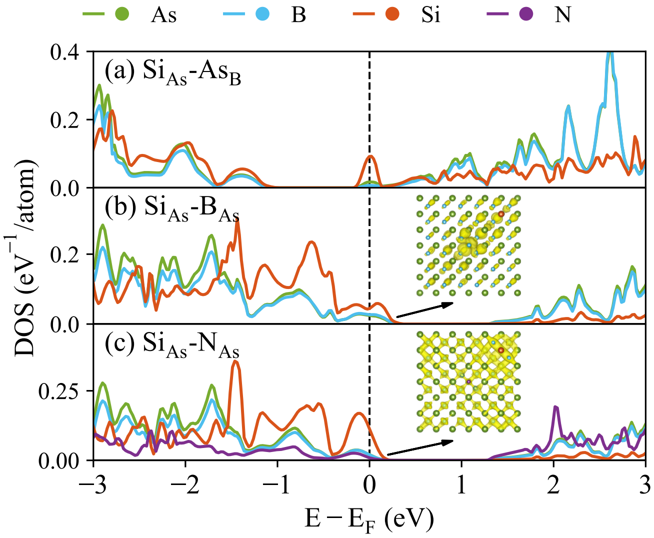

FIG. S3. Calculated electronic DOS of $\mathrm{Si_{As}}$-doped BAs in the presence of (a) $\mathrm{As_B}$, (b) $\mathrm{B_{As}}$, and (c) $\mathrm{N_{As}}$ point defect. The inset figures show the isosurfaces of charge density near VBM (<0.1eV) or within the band gap.

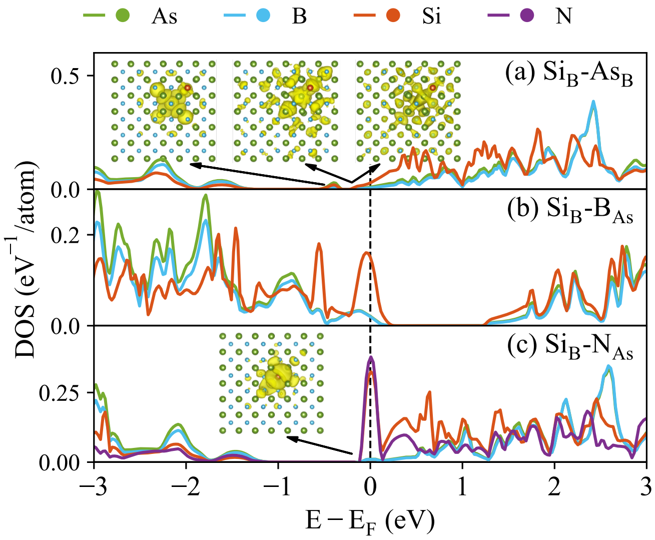

FIG. S4. Calculated electronic DOS of Si$_B$-doped BAs in the presence of (a) As$_B$, (b) B$_{As}$, and (c) N$_{As}$ point defect. The inset figures show the isosurfaces of charge density near CBM (<0.1eV) or within the band gap.

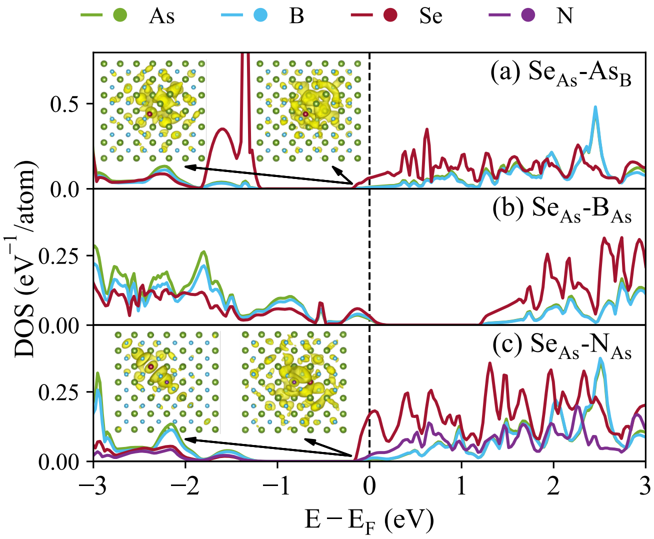

FIG. S5. Calculated electronic DOS of Se$_{As}$-doped BAs in the presence of (a) As$_B$, (b) B$_{As}$, and (c) N$_{As}$ point defect. The inset figures show the isosurfaces of charge density near CBM (<0.1eV) or within the band gap.

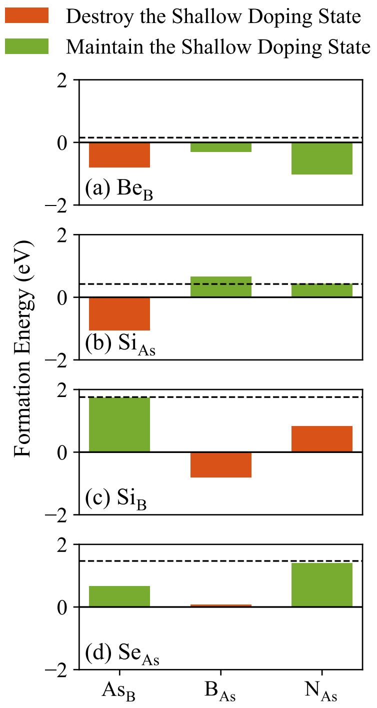

FIG. S6. Calculated formation energy of (a) Be_B, (b) Si_{As}, (c) Si_B, and (d) Se_{As} dopants in the presence of selected point defects. The dashed lines represent formation energy of dopants without point defects. The green color signifies that the shallow doping state is preserved as the dopants in pristine BAs, whereas the red color indicates otherwise.

V. ISOSURFACES OF CHARGE DENSITY

In this section we provide enlarged figures of isosurfaces of charge density, for all bands near CBM or VBM (<0.1 eV) and within the band gap. In each case, from left to right, the energies of electronic bands are arranged from small to large values, indicating that the band indexes also increase from small to large values.

A. Dopants

$\mathrm{Be_B}$: A three-fold degenerated band at VBM

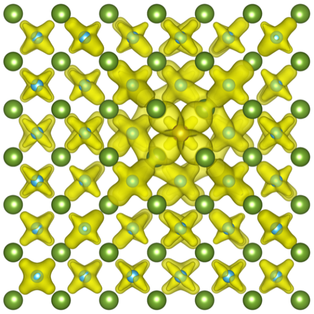

$\mathrm{Si_{As}}$: A three-fold degenerated band at VBM

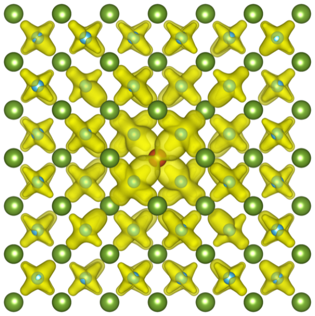

$\mathrm{Si_B}$: Two bands near CBM

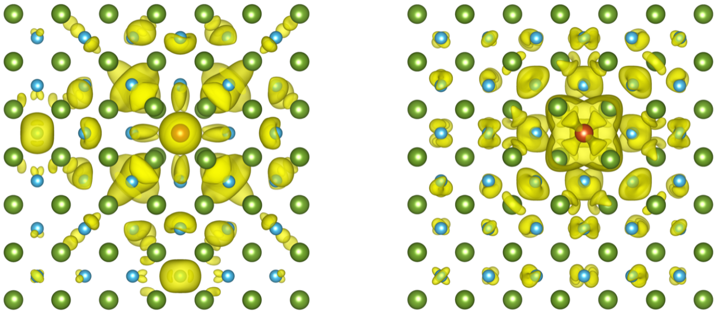

$\mathrm{Se}_{\mathrm{As}}$: Two bands near CBM

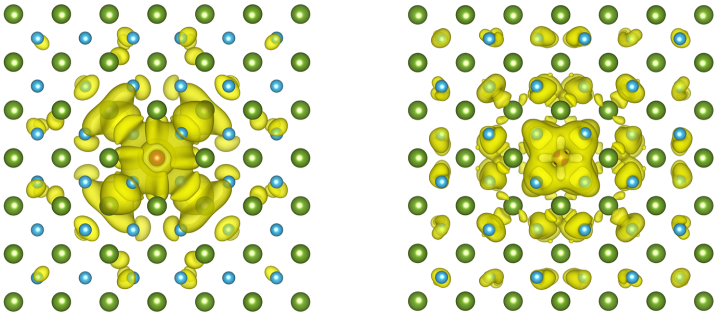

B. Dopants with point defects

Be_{B}-$\mathrm{As}_{\mathrm{B}}\mathrm{B}_{\mathrm{As}}$: Three bands near VBM

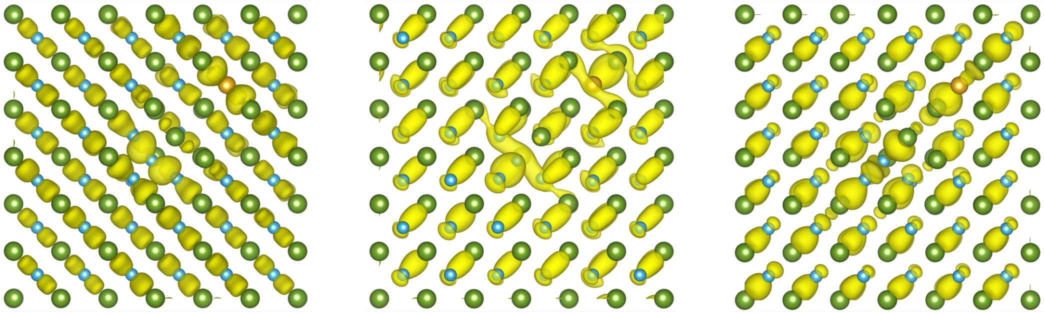

Be_{B}-C_{As}: One band near VBM:

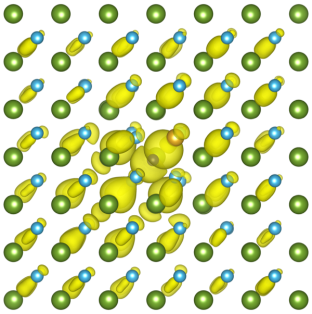

Be_{B}-$\mathrm{O}_{\mathrm{B}}\mathrm{O}_{\mathrm{As}}$: One band at VBM, and one band at CBM

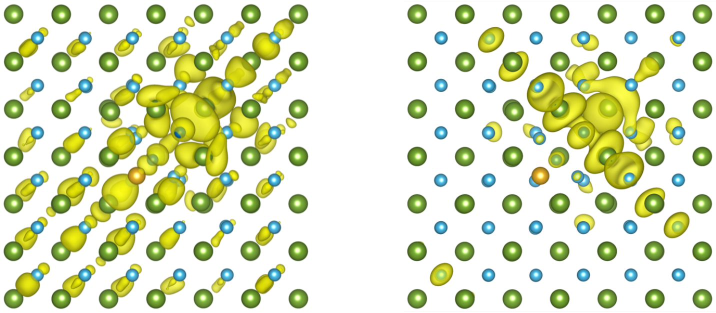

Be$_{\mathrm{B}}$-Si$_{\mathrm{As}}$: Three bands near VBM

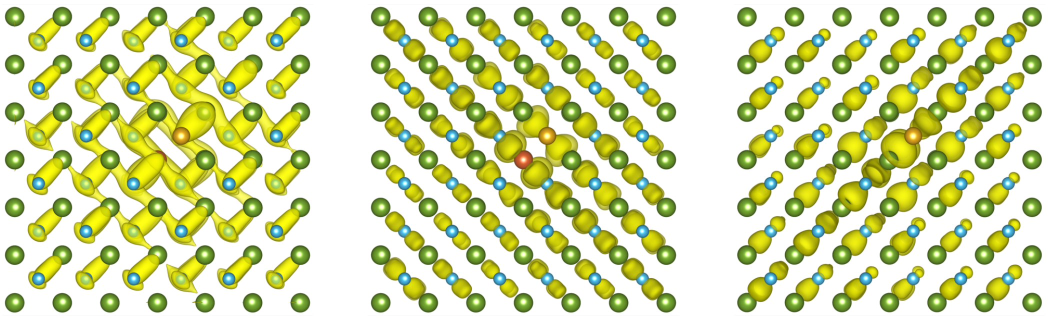

Be$_{\mathrm{B}}$-C$_{\mathrm{As}}$Si$_{\mathrm{B}}$: Three bands near VBM

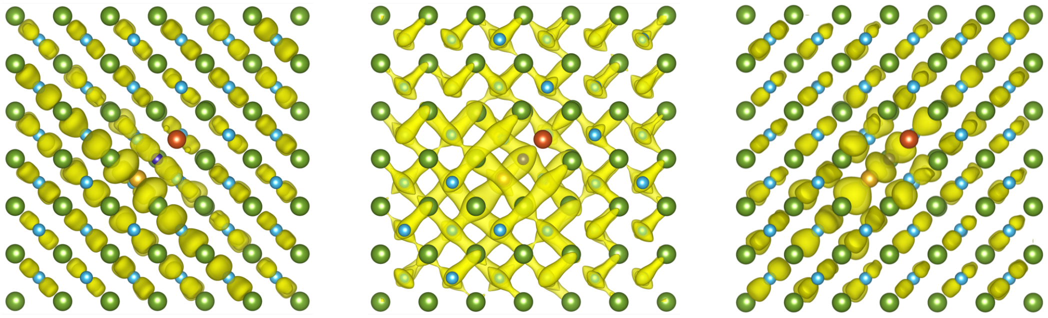

Be$_{\mathrm{B}}$-O$_{\mathrm{B}}$Si$_{\mathrm{As}}$: One band at VBM, and one band in the band gap

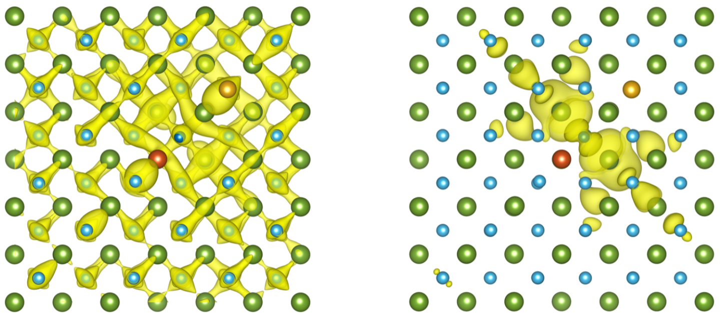

Be$_{\mathrm{B}}$-B$_{\mathrm{As}}$: One two-fold degenerated band at VBM, and one band in the band gap

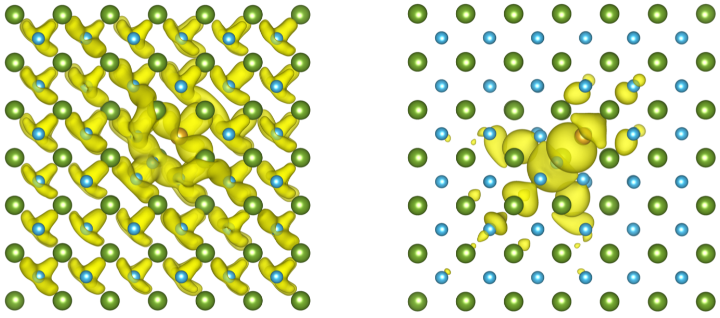

$\mathrm{Be_B}$-$\mathrm{N_{As}}$: One band near VBM, and one two-fold degenerated band at VBM

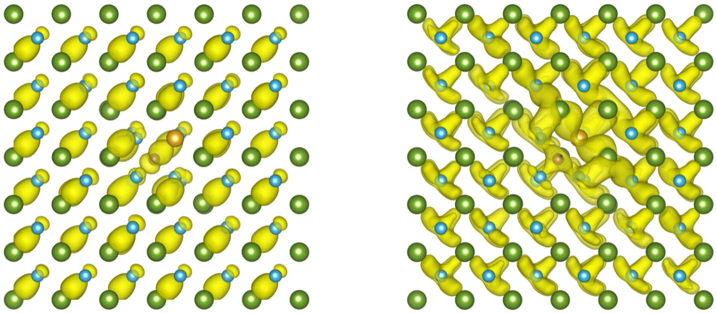

$\mathrm{Si_{As}}$-$\mathrm{As_B B_{As}}$: Three bands near VBM

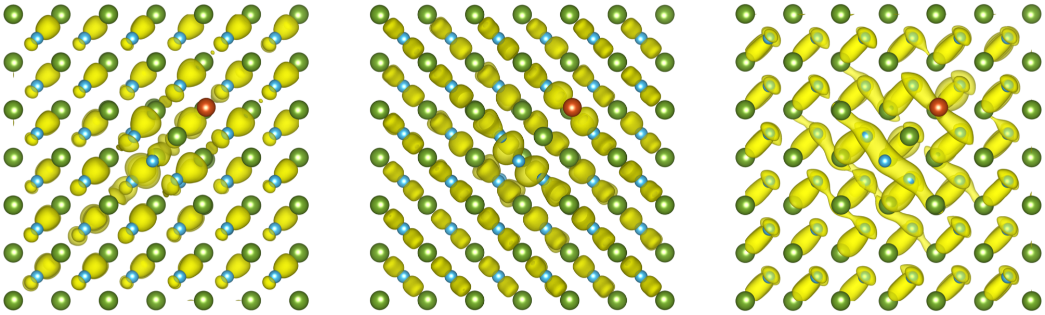

$\mathrm{Si_{As}}$-$\mathrm{C_{As}}$: Three bands near VBM

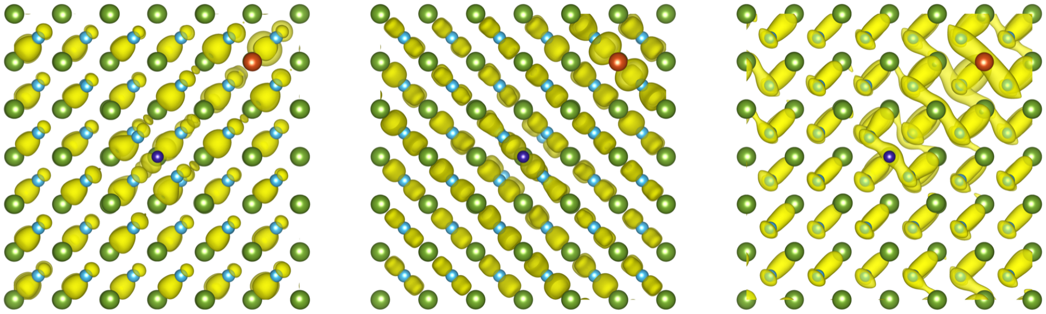

$\mathrm{Si_{As}}$-$\mathrm{O_B O_{As}}$: One band in the band gap

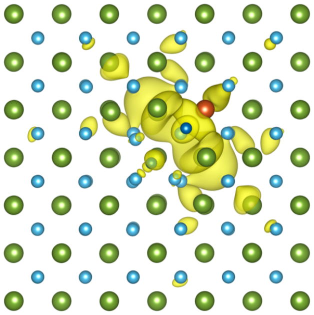

Si$_{\mathrm{As}}$-C$_{\mathrm{As}}$Si$_{\mathrm{B}}$: Three bands near VBM

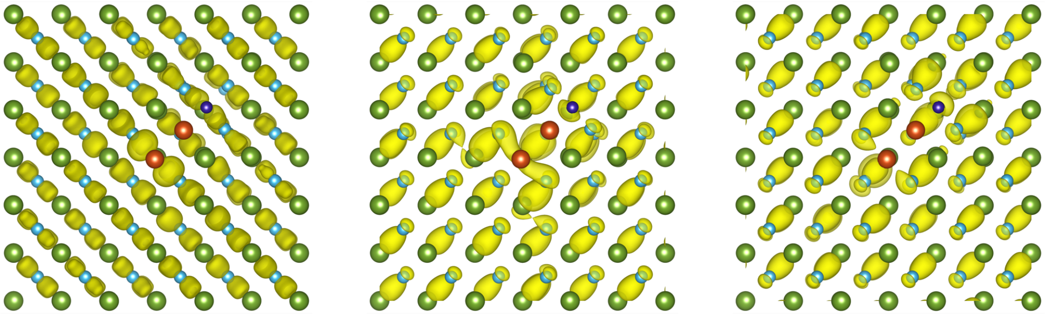

Si$_{\mathrm{As}}$-O$_{\mathrm{B}}$Si$_{\mathrm{As}}$: Two bands at VBM, and one band in the band gap

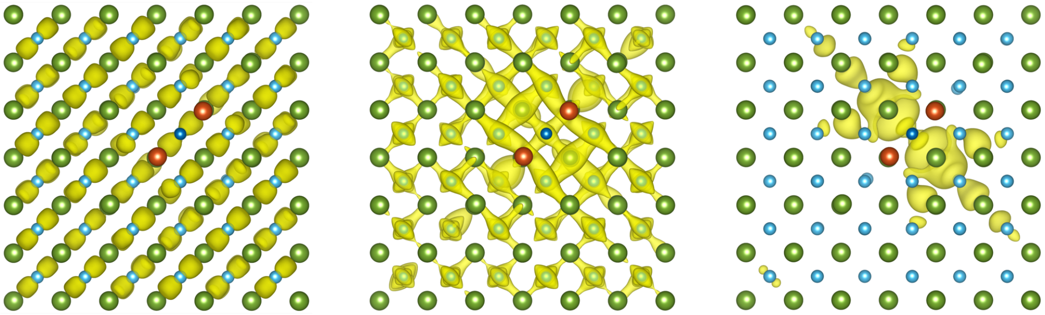

Si$_{\mathrm{As}}$-B$_{\mathrm{As}}$: Three bands near VBM

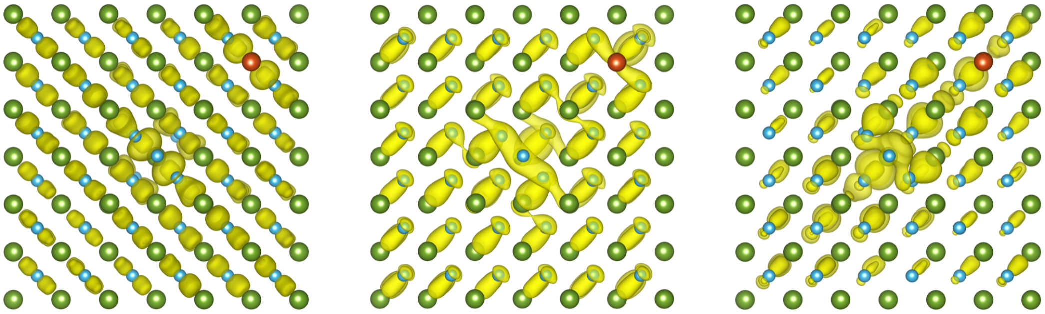

Si$_{\mathrm{As}}$-N$_{\mathrm{As}}$: Three bands near VBM

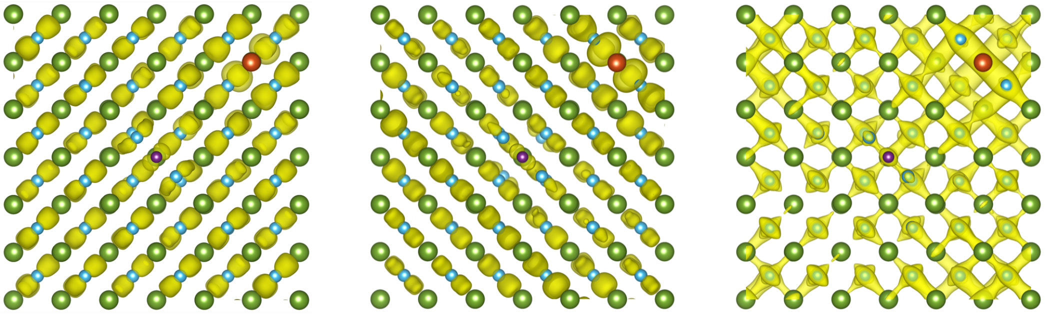

$\mathrm{Si_B}$-$\mathrm{As_B B_{As}}$: Two bands near CBM

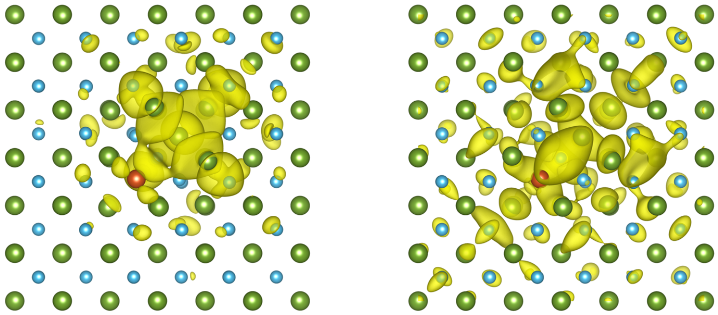

$\mathrm{Si_B}$-$\mathrm{O_B O_{As}}$: One band in the band gap

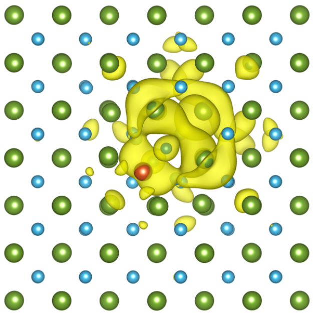

$\mathrm{Si_B}$-$\mathrm{C_{As} Si_B}$: Two bands near CBM

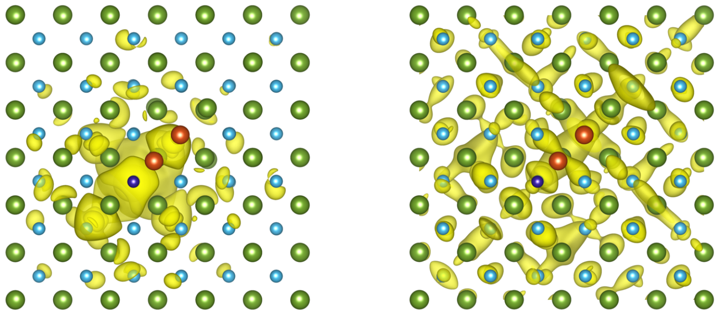

$\mathrm{Si_B}$-$\mathrm{O_B Si_{As}}$: One band in the band gap

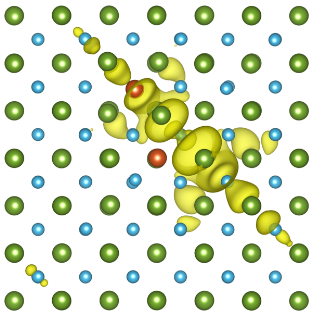

$\mathrm{Si_B}$-$\mathrm{As_B}$: One band in the band gap, and two bands near CBM

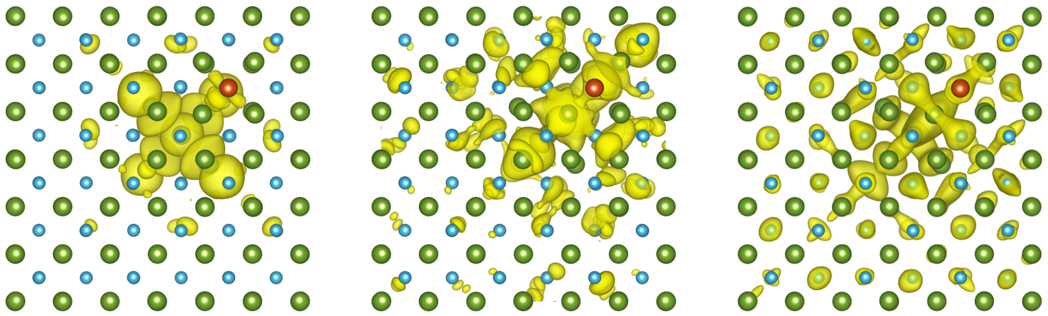

$\mathrm{Si_B}$-$\mathrm{N_{As}}$: One band at CBM

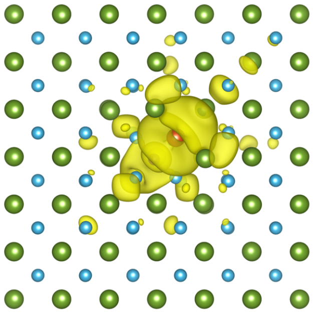

$\mathrm{Se_{As}}$-$\mathrm{As_B B_{As}}$: Two bands near CBM

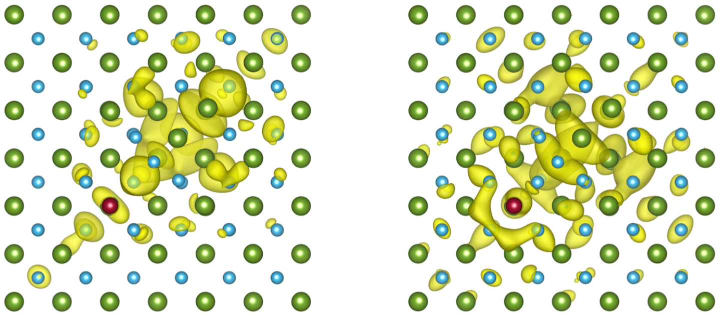

$\mathrm{Se_{As}}$-$\mathrm{O_B O_{As}}$: One band in the band gap

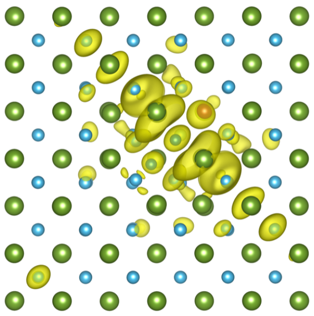

$\mathrm{Se_{As}}$-$\mathrm{C_{As}Si_{B}}$: Two bands near CBM

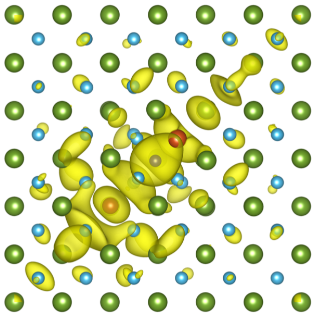

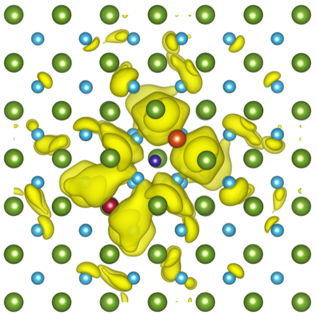

$\mathrm{Se_{As}}$-$\mathrm{O_{B}Si_{As}}$: One band in the band gap

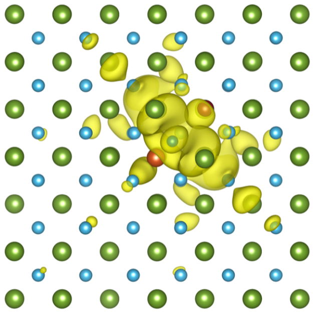

$\mathrm{Se_{As}}$-$\mathrm{As_{B}}$: Two bands near CBM

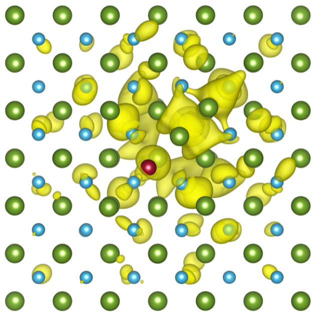

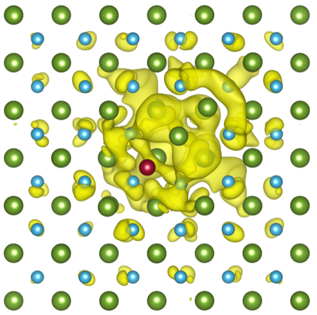

$\mathrm{Se_{As}}$-$\mathrm{N_{As}}$: Two bands near CBM

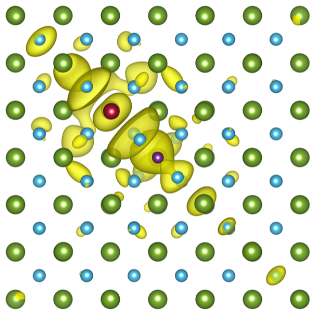

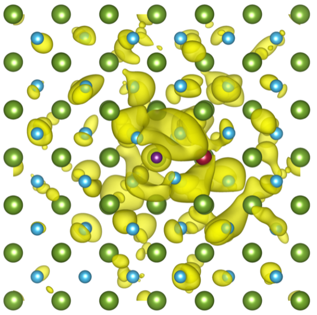

[1] C. Freysoldt, J. Neugebauer, and C. G. Van de Walle, Physical Review Letters **102**, 016402 (2009).
[2] S. Chae, K. Mengle, J. T. Heron, and E. Kioupakis, Applied Physics Letters **113**, 212101 (2018).
[3] J. L. Lyons, J. B. Varley, E. R. Glaser, J. A. Freitas, Jr., J. C. Culbertson, F. Tian, G. A. Gamage, H. Sun, H. Ziyaee, and Z. Ren, Applied Physics Letters **113**, 251902 (2018).
[4] J. Buckeridge and D. O. Scanlon, Physical Review Materials **3**, 051601 (2019).